

Realization of a nanoscale magnonic directional coupler for all-magnon circuits

Q. Wang¹, M. Kewenig¹, M. Schneider¹, R. Verba², B. Heinz^{1,3}, M. Geilen¹, M. Mohseni¹, B. Lagel⁴,
F. Ciubotaru⁵, C. Adelman⁵, C. Dubs⁶, P. Pirro¹, T. Bracher¹, and A. V. Chumak¹

¹*Fachbereich Physik and Landesforschungszentrum OPTIMAS, Technische Universitat Kaiserslautern, D-67663 Kaiserslautern, Germany*

²*Institute of Magnetism, Kyiv 03142, Ukraine*

³*Graduate School Materials Science in Mainz, Staudingerweg 9, 55128 Mainz, Germany*

⁴*Nano Structuring Center, Technische Universitat Kaiserslautern, D-67663 Kaiserslautern, Germany*

⁵*Imec, B-3001 Leuven, Belgium*

⁶*INNOVENT e.V., Technologieentwicklung, Prussingstrae 27B, 07745 Jena, Germany*

Abstract

Magnons are of great interest as data carriers in future low-energy computing devices. The main challenge is the realization of an integrated magnonic circuit. Such a circuit requires the development of a universal reconfigurable unit for performing different logic operations. Moreover, a condition for the cascading of multiple units, while all the information is kept within the magnonic domain, is a nonlinear functionality of the unit. Here, we report on the experimental realization of a nanoscale magnonic directional coupler which fulfills all these criteria. Data is coded into the spin wave amplitude and is guided towards one of its two outputs depending on the signal frequency, magnitude, and on the magnetic field. By controlling these degrees of freedom, the multi-functionality and reconfigurability of the device is achieved. The operation of the directional coupler as a multiplexer, fan-out, AND, and XOR logic gates, as well as a half-adder, is demonstrated.

The field of magnonics [1-6] proposes a promising approach for more-than-Moore computing, in which magnons, the quanta of spin waves, carry the information instead of electrons [6-9]. The phase of a spin wave provides an additional degree of freedom to use efficient computing concepts resulting in a valuable decrease in the footprint of logic units [3, 6-9]. Additional advantages of magnonics are the scalability of magnonic structures down to the nanometer regime [10-12] and the possibility to operate with spin waves of nanometer wavelength [13-17]. The further miniaturization will, consequently, result in an increase in the frequency of spin waves used in the devices from the currently employed GHz range up to the THz range [18-21]. Additional important features, which are provided by spin waves, are the low-loss information transfer [22-25] and abundant nonlinear spin wave phenomena [26-30]. Just recently a set of magnon-based data processing units was successfully demonstrated: Spin wave logic gates [31,32], majority gates [3,7,33], magnon transistors and valves [28,34], spin wave multiplexers [35,36], a magnonic half-adder [30], and unconventional and neuromorphic computing elements [37-40].

The next major challenge in magnon-based computing is the transition from a single logic unit to an integrated circuit. As an alternative to approaches relying on the conversion between electric signals and magnons [1, 6-8], an all-magnon approach [28] allows for logic operations purely in the magnonic domain. The initial step in the development of an integrated magnonic circuit was taken recently by numerical simulations, and an integrated magnonic half-adder was predicted [30]. The essential part of the half-adder is a directional coupler, which was first investigated by Sadovnikov *et al.* [41] at the macroscale and, further, numerically by Wang *et al.* at the nanoscale [42]. The directional coupler is of exceptional importance since it simultaneously serves as a magnonic conduit and splitter replacing 3D bridges in circuits [42] and providing the nonlinear switching functionality needed for logic functions [30]. In the following, we demonstrate the realization of such a nanoscale directional coupler and investigate its functionality using space-resolved micro-focused Brillouin Light Scattering (μ BLS) spectroscopy.

Frequency-dependent guiding of the spin wave signal

Figure 1a presents a Scanning Electron Microscopy (SEM) image of the nanoscale directional coupler fabricated from an 85 nm thick Yttrium Iron Garnet (YIG) film grown by liquid phase epitaxy on a Gadolinium Gallium Garnet (GGG) substrate [23] (see Methods). The two spin wave waveguides, each of 350 nm width, are physically separated by a gap of 320 nm. In order to transfer spin waves out of the directional coupler into an “isolated” conduit, the gap between the waveguides gradually increases by two 12-degree bent waveguides until it reaches a constant gap of 1.32 μ m. Such a large gap ensures the decoupling of the waveguides and allows for the independent transfer of the spin wave signal from both outputs to a consequent magnonic device. A 200 nm thick U-shaped gold antenna consisting of two 500 nm wide strips with 1 μ m edge-to-edge separation is placed on top of one YIG waveguide to excite spin waves.

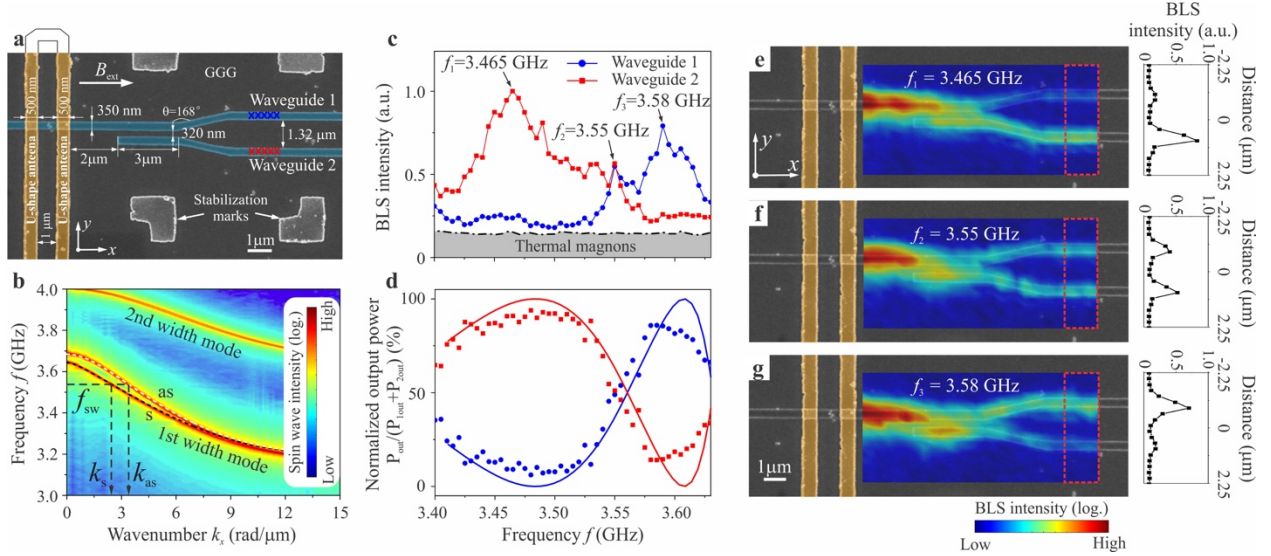


Fig. 1. Sample geometry and working principle of the directional coupler. **a.** SEM image of the directional coupler (shaded in blue) with the U-shaped antenna. **b.** Spin wave dispersion relation of the first two width modes obtained using micromagnetic simulation (color-code) and analytic theory (dashed lines). YIG waveguides of 350 nm width and 320 nm gap in between are considered. **c.** Averaged spin wave spectra measured by μ BLS spectroscopy on the first (blue circles) and on the second (red squares) output waveguide. The arrows indicate the frequencies, which are chosen for the demonstration of different functionalities of the directional coupler in Fig. 1e-g. External magnetic field $B_{\text{ext}} = 56$ mT and microwave power $P_{\text{RF}} = 0$ dBm. **d.** The frequency dependence of the normalized output powers $P_{\text{out}}/(P_{1\text{out}}+P_{2\text{out}})$ with subtracted thermal background for both waveguides. Circles and squares represent experimental results and solid lines are theoretical calculations of the normalized output spin wave intensity at the first (blue) and the second (red) output waveguide. **e-g.** Two-dimensional BLS maps (the laser spot was scanned over an area of $9.4 \times 4.5 \mu\text{m}^2$ by 30×20 points) of the BLS intensity for **e.** $f_1 = 3.465$ GHz, **f.** $f_2 = 3.55$ GHz, and **g.** $f_3 = 3.58$ GHz. The right panels show the spin wave intensity integrated over the red dashed rectangular regions at the end of the directional coupler.

The U-shape allows for a better confinement of the microwave fields due to the counter-propagating currents in the adjacent metallic strips, reducing spurious excitation far away from the antenna. The distance to the second waveguide is $2 \mu\text{m}$ which is, thus, sufficient to avoid any sizable direct spin wave excitation in it.

An external magnetic field $B_{\text{ext}} = 56$ mT is applied along the YIG conduits (x -axis) to saturate the directional coupler in a backward volume waves geometry [9] and a radio-frequency (RF) current with power $P_{\text{RF}} = 0$ dBm is applied to the antenna in order to excite spin waves. To detect the spin wave intensity in the nanoscale directional coupler, space-resolved μ BLS spectroscopy is used [43] (see Methods). As a first step, we investigate five points along each output waveguide as marked by blue and red crosses in Fig. 1a. Figure 1c shows the spin wave intensities for the two output waveguides averaged over these points as a function of the excitation frequency. As it can be seen, the two spectra show quite different features:

In the first waveguide, the maximum spin wave intensity was observed at 3.58 GHz. In contrast, the maximum intensity in the second waveguide was found around 3.465 GHz and only very weak spin wave intensities are detected above 3.575 GHz.

To understand the nature of this frequency separation, the dispersion relations of the first two spin wave width modes for coupled waveguides are shown in Fig. 1b. The color coding represents the results of micromagnetic simulations, whereas the dashed lines are calculated using the analytical theory [12,42] (see Methods). The dispersion curve of the first width mode splits into antisymmetric (as) and symmetric (s) modes due to the dipolar interaction between the waveguides. This results in an oscillation of the spin wave energy between the coupled waveguides [41,42]. Thus, once the spin wave energy is injected into only one of the waveguides, it will be transferred completely to the other one after the propagation of a certain distance which is called coupling length L . The coupling length L is defined by the wave numbers of the spin wave modes k_{as} and k_s : $L = \pi / \Delta k = \pi / |k_{as} - k_s|$ and depends strongly on the spin wave frequency and other parameters [42]. Since the length of the coupled waveguides is fixed, the ratio of this length to the coupling length L defines into which of the two output waveguides of the directional coupler the spin wave will be guided [42].

Figure 1d shows the frequency dependence of the normalized output spin wave intensities for both output waveguides. Experimental data are well fitted by the analytical model, presented in Methods. Compared to the standard theory [42], which accounts for the coupling of the straight part of waveguides, the presented model is improved by taking into account an additional “diagonal” coupling present prior to the geometrical start of the second waveguide as well as the coupling between the bent waveguides (see Fig. 1a). These additional couplings are of importance because of the relatively large minimal gap between the waveguides leading to a relatively weak “main” coupling in the straight region. The first mechanism of the additional coupling, which is described by a phenomenological fitting parameter in Methods, strongly depends on the spin wave wavelength and is pronounced only for the long waves having frequencies above 3.50 GHz. For shorter waves rigorous theory works well despite the fact that any rough edges and the non-rectangular shape of the cross-section of the fabricated waveguides [12] are not taken into account. This is an indication of the high robustness of the proposed directional coupler design. The measured maximal transfer of the spin wave energy takes place at a spin wave frequency of around 3.48 GHz and is equal to 93.8% which is only slightly below the theoretical value of 100%. This difference is likely due to imperfections of the fabricated structure (not identical waveguides) and might be decreased by the further improvement of the nanostructuring process or by the optimization of the directional coupler design.

Two-dimensional BLS spectroscopy scans of the spin wave intensity are shown in Fig. 1(e-g) to directly demonstrate the functionality of the directional coupler. Figure 1e shows the case when spin waves are excited in the first waveguide at a frequency of $f_1 = 3.465$ GHz and most of the energy is transferred to

the second waveguide. Thus, this planar two-dimensional directional coupler can be used to efficiently connect two magnonic conduits without the need for complex and costly three-dimensional bridges which are used in modern electronic circuits [42]. Figure 1g shows an entirely different spin wave path in the directional coupler. The increase in the spin wave frequency up to $f_3 = 3.58$ GHz results in a decrease of the coupling length L by roughly a factor of two. As a result, the spin wave transfers all its energy from the first waveguide to the second one and back. Thus, 86% of the total spin wave energy is guided back into the first output waveguide of the directional coupler. This demonstrates the potential use of the directional coupler as a frequency division demultiplexer: If different frequencies are applied to the same input of the directional coupler, they will be transferred to the different outputs of the device. Finally, Fig. 1f demonstrates that the directional coupler can also be used as a 50/50 power splitter in which half of the spin wave energy is transferred to the second waveguide and half of it remains in the first one.

It should be emphasized that such an efficient guiding of spin waves in the bent waveguides and the excellent operational characteristics of the directional coupler are only possible due to the nanoscopic sizes of the YIG waveguides. The decrease in the dimensions from the micro- to the nanoscale results, first of all, in a single-mode operational regime since the higher thickness and width modes have considerably higher frequencies (see Fig. 1c). Thus, the elastic scattering of spin waves into these modes, having different coupling strength [41,44], is prohibited. Moreover, the nanoscaling solves the problem of anisotropic spin wave dispersions [9] since in a self-biased nanoscopic waveguides a spin wave always propagates along the magnetization orientation.

Field-dependent guiding of the spin wave signal

One of the most significant advantages of spin wave directional couplers is their (re-)configurability via the magnetic field or magnetization orientation that allows to change the functionality while conserving the frequency of the signal [42]. To demonstrate this feature, Fig. 2a shows the output spin wave intensity for a frequency of $f_1 = 3.465$ GHz as a function of the applied external magnetic field at the output waveguides 1 and 2. Figure 2b presents the experimental and theoretical field dependencies of the normalized spin wave intensity at the outputs. It can be seen from both figures that the variation of the applied field can tune the distribution of the spin wave energy between the output waveguides. This is due to the fact that the coupling length L is strongly dependent on the spin wave wavelength which is defined by the applied field at constant spin wave frequency. For the field $B_{\text{ext}} = 56$ mT, the spin wave energy is transferred to the second output waveguide, as shown in Fig. 2c. When the external field is decreased to 53.2 mT, the coupling length decreases due to a downward shift of the spin wave dispersion curve and the directional coupler works as a 50/50 power splitter (see Fig. 2d). Such a splitter can also be used as a fan-out logic gate if parametric pumping or spin transfer torque (STT) amplifier [6] will be installed at the

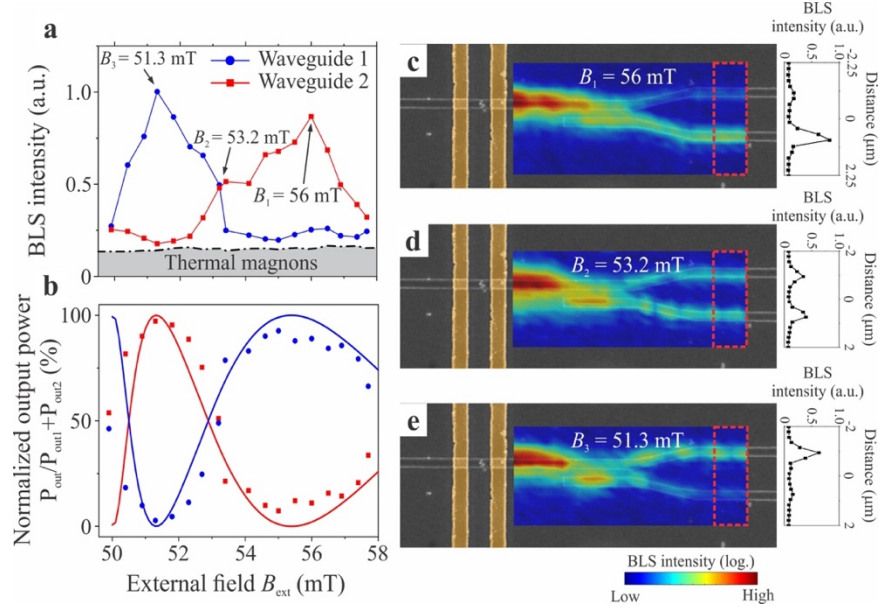


Fig. 2. Reconfigurability of the directional coupler by an applied magnetic field. *a.* The averaged spin wave intensity for a frequency of 3.465 GHz as function of the external field for the first (blue circles) and the second (red squares) output waveguide of the directional coupler. *b.* Measured (circles and squares) and theoretically calculated (solid lines) normalized output spin wave intensities at the first (blue) and second (red) output waveguide for different external fields. *c-e.* Two-dimensional BLS maps of the spin wave intensity for the different external magnetic fields: *c.* $B_1 = 56$ mT, *d.* $B_2 = 53.2$ mT, and *e.* $B_3 = 51.3$ mT. The right panels show the spin wave intensity integrated over the red dashed rectangular regions.

outputs of the device to compensate the split in energy. A further decrease of the external field to 51.3 mT results in a further decrease of the coupling length and most of the spin wave energy is transferred back to the first waveguide as it is shown in Fig. 2e. Thus, the directional coupler can act as a signal multiplexer since its output configuration can be switched from one output to another within a small field range of only $\Delta B_{\text{ext}} = 4.7$ mT. In future circuits, an electric current applied to a metallic strip could be used to create a local Oersted field and to realize a switching of the directional coupler output via electric current control [45]. As an energy-efficient alternative, a magnetic field from switchable nanosized magnets [46] could be used to realize a non-volatile reconfigurability of the directional coupler.

Nonlinear functionality of the magnonic directional coupler

As already mentioned, a large benefit of spin waves is their pronounced natural nonlinearity that allows for an all-magnon control of one magnonic unit by another. In our studies, the phenomenon of nonlinear shift of the dispersion relation [27, 30] is used in contrast to the multi-magnon scattering exploited in the realization of a magnon transistor [28]. In the relatively weak nonlinear regime, where the dipolar coupling between the waveguides is larger than nonlinear frequency shift of spin waves, the nonlinear

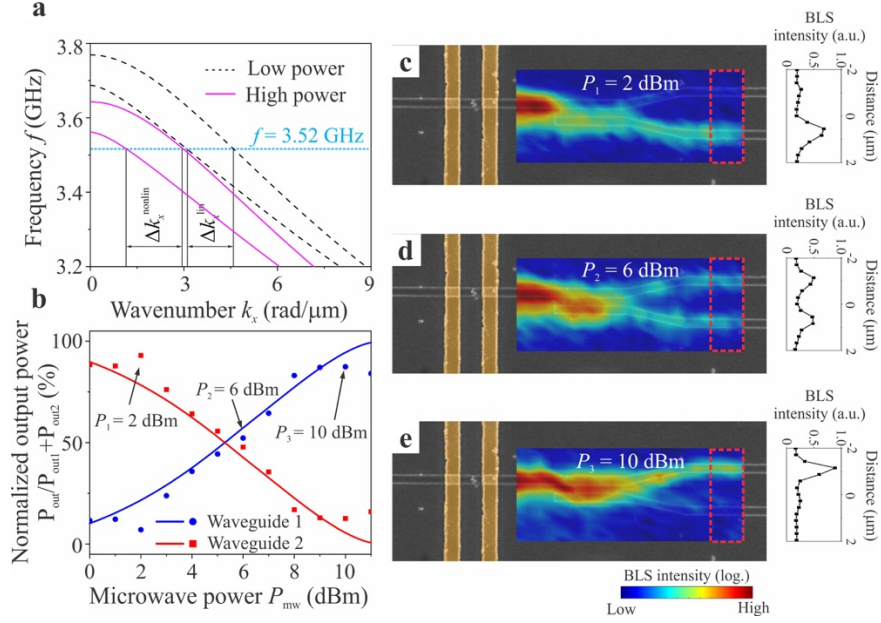


Fig. 3 Nonlinear functionality of the directional coupler. **a.** The dispersion relations of symmetric and asymmetric spin wave modes in the coupled waveguides for low (black dashed lines) and high (magenta solid lines) powers. The increase in spin wave amplitude results in the downshift of the dispersion curves. **b.** Averaged spin wave intensity as a function of the microwave power P_{RF} . **c-e:** Two-dimensional BLS maps of the spin wave intensity for a frequency of $f = 3.52$ GHz and different input powers **c.** $P_1 = 2$ dBm, **d.** $P_2 = 6$ dBm, and **e.** $P_3 = 10$ dBm. The right panels show the spin wave intensity integrated over the regions indicated by red dashed rectangular regions.

operation of directional coupler can be described simply by taken into account nonlinear frequency shift of symmetric and antisymmetric collective modes, the same for both and equal to the nonlinear frequency shift of waves in isolated waveguides [30,47]:

$$f_{s,as}^{(nl)}(k_x, a_{k_x}) = f_{s,as}^{(0)}(k_x) + T_{k_x} |a_{k_x}|^2, \quad (1)$$

where $f_{s,as}^{(0)}(k_x)$ are the dispersion relations of symmetric and antisymmetric modes of the coupled waveguides in the linear region, a_{k_x} is the canonical spin wave amplitude and T_{k_x} is the nonlinear shift coefficient. For the backward volume geometry, the nonlinear shift coefficient is negative [27,30,47] and, thus, the spin wave dispersion curves shift down with an increase in the spin wave amplitude defined by the applied RF power. The calculated spin wave dispersions are shown in Fig. 3a for low and high applied microwave powers (see Methods). As can be seen in the figure, for a fixed spin wave frequency of 3.52 GHz, the coupling length L decreases from $\pi/\Delta k_x^{\text{lin}}$ to $\pi/\Delta k_x^{\text{nonlin}}$ with an increase in input power, resulting in changed device characteristics.

To study the nonlinear switching functionality of the presented directional coupler, the constant external magnetic field $B_{\text{ext}} = 56$ mT and the RF frequency $f = 3.52$ GHz were applied, while the microwave power P_{RF} was varied in the range from 0 dBm to 11 dBm. Figure 3b shows the normalized spin wave intensity at the output waveguides 1 and 2 as a function of the microwave power. The result clearly shows that the respective output spin wave intensity strongly depends on the input microwave power due to the nonlinear effects. Figure 3c shows that for a relatively low input power $P_{\text{RF}} = 2$ dBm, the output spin wave energy is transferred to the second waveguide. This regime can be considered as a linear one. For the increased input power of $P_2 = 6$ dBm, the spin wave dispersion shift implies that at this power, half of the output spin wave energy is transferred back to the first waveguide and the directional coupler, thus, works as a 50/50 splitter. A further increase of the input power up to 10 dBm results in a further dispersion shift, an decrease of the coupling length L and in a transfer of the spin wave energy back to the first waveguide as it can be seen in Fig. 3e. As it can be seen in Fig. 3b, the developed theoretical model (see Methods) fits the experimental data well for the applied powers below 10 dBm. For the higher powers, higher-order nonlinear effects should be taken into account additionally [48].

Nonlinear directional coupler for half-adder functionality

In the final part, we would like to discuss the application of the reported nanoscale magnonic directional coupler for the realization of a half-adder which is a primary component of any arithmetic logic system. Figure 4a shows a general schematic layout of the half-adder in electronics which combines XOR and AND logic gates using a three-dimensional bridge consisting of 14 transistors (assuming 8 transistors for XOR and 6 for AND gates). It adds two single binary digital Inputs “ A ” and “ B ” and has two Outputs Carry (“ C ”) and Sum (“ S ”). The truth table of a half-adder is shown in Fig. 4b. The magnonic half-adder was proposed numerically in Ref. [30]. In this study, the inputs of the half-adder were mixed together using one directional coupler operating in a linear regime and were applied to a second directional coupler with stronger coupling coefficient to perform the nonlinear switch operation. To demonstrate that the reported here directional coupler can work be a central component of a half-adder, the first spin wave coupler was replaced by a microwave directional coupler and two microwave signals “ A ” and “ B ” were mixed together instead of two magnon signals, where the phase of Input “ B ” is shifted by $\pi/2$ with respect to the phase of Input “ A ”. One of the output ports of the microwave directional coupler is then connected directly to the U-shaped antenna to excite spin waves in the magnonic directional coupler as it is shown in Fig. 4c.

Let us first consider the case of logic Inputs “ A ”=“0” and “ B ”=“0” when no microwave power is sent to magnonic directional coupler and only thermal magnons are detected at the output waveguides. The normalized BLS counts, which are proportional to the measured spin wave intensity, are shown in the “Output” columns of the table in Fig. 4d. In the following, any spin wave intensity below a threshold value

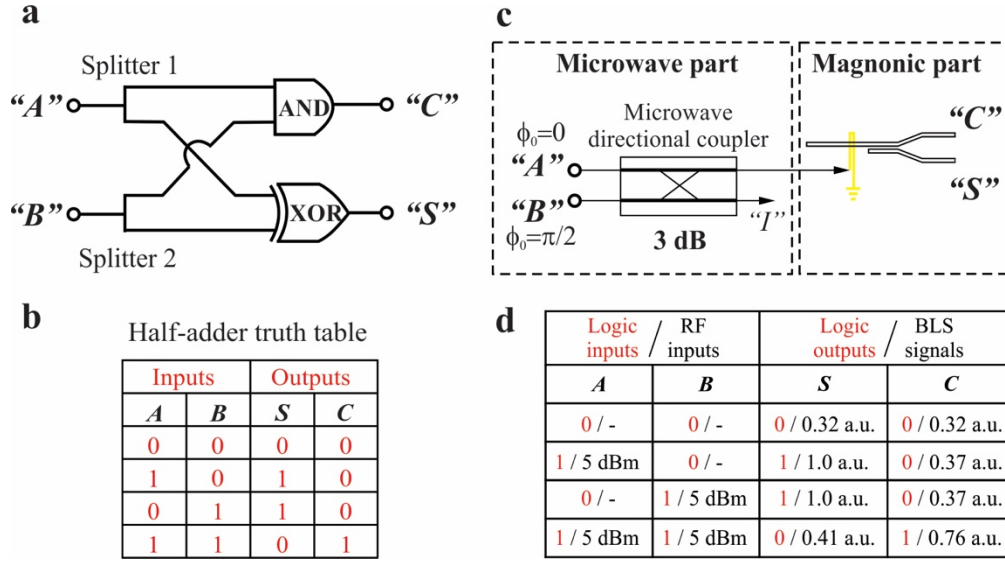


Fig. 4. Half-adder functionality of the directional coupler. a. Sketch of half-adder schematics in electronics. b. Half-adder truth table. c. Magnonic directional coupler with microwave inputs applied via a microwave directional coupler. d. Magnonic half-adder truth table with experimental results. The logic inputs and applied microwave powers are shown in the “Input” columns. The logic outputs and normalised BLS intensity are shown in the “Output” columns. The spin wave intensity below a threshold value of 0.5 is considered to be logic “0” and above it is logic “1”.

of 0.5 is considered to be logic “0” and above this value to be logic “1”. Thus, logic Inputs “*A*”=“0” and “*B*”=“0” correspond to the logic Outputs “*S*”=“0” and “*C*”=“0”. The application of 5 dBm microwave power to the Input “*A*” corresponds to the case “*A*”=“1” and “*B*”=“0”. In this case, the input power is split by the microwave directional coupler into two equal parts of 2 dBm power each. One of them is used to excite spin waves and most of the spin wave energy is transferred to the second spin wave waveguide as was shown in Fig. 3c realizing the case of logic Outputs “*S*”=“1” and “*C*”=“0”. If a signal of 5 dBm power is applied to Input “*B*”, the situation is practically identical as it can be seen in the table. However, the situation is different, if the input powers applied to “*A*” and “*B*” are both 5 dBm (“*A*”=“1” and “*B*”=“1”). The phase shift of output “*B*” results in the guiding of both microwave signals to the first output of the microwave directional coupler and, consequently, in a microwave power of 8 dBm applied to the magnon directional coupler. It can be seen from Fig. 3a that most of the spin wave energy is transferred back to the first waveguide and the case “*S*”=“0” and “*C*”=“1” is realized. Thus, the whole truth table of a half-adder is fulfilled. The signal to noise ratio of the device can be increased by further optimization of the parameters of the magnonic directional coupler.

The above logic elements are cascable and can therefore be used to design any logic circuit in combination with spin wave amplifiers. For example, as it was discussed in Ref. [30], the spin wave signal from the Output “*C*” (AND logic gate) of a magnonic half-adder can be directly sent to the input of a next

logic unit while the signal from the Output “ S ” (XOR logic gate) has first to be amplified four times. The proposed fan-out logic gate also requires amplification to compensate for the splitting of the energy. Energy efficient approaches to realize such amplifiers are parametric pumping [2, 9, 40, 47] and STT-based techniques [6, 9, 22], which together with directional couplers thus form a set of universal building blocks for magnonic logic.

In summary, a fully functional nanoscale spin wave directional coupler was fabricated and studied experimentally using μ BLS spectroscopy. The results were supported by numerical simulations and the developed analytical theory. It is shown that the spin wave energy can be guided to different outputs depending on the applied microwave frequency or controlled by a small variation of an applied magnetic field of about 5 mT. Thus, it is proven that the directional coupler is a universal reconfigurable multifunctional device which can be used to process analogue and digital information as microwave filter, power splitter for fan-out logic gates, frequency division or signal multiplexer and as a planar interconnecting element for magnonic conduits. Furthermore, the nonlinear functionality of the directional coupler to switch the output by changing the spin wave amplitude was demonstrated. Particularly, this ability opens a path for the realization of all-magnon integrated circuits in which data will be processed purely within the magnonic domain without the use of electric currents. As an example, it was shown that the reported directional coupler performs AND and XOR logic operations and can be the central component of a wave-based half-adder that can elegantly replace the needed 14 transistors in modern CMOS technology due of its simplicity.

Acknowledgements:

The authors thank Burkard Hillebrands for support and valuable discussions. This research has been supported by ERC Starting Grant 678309 MagnonCircuits, FET-OPEN project CHIRON (contract number 801055), by the DFG through the Collaborative Research Center SFB/TRR-173 “Spin+X” (Projects B01) and through the Project DU 1427/2-1. R. V. acknowledges support from the Ministry of Education and Science of Ukraine, Project 0118U004007.

References

- 1 Kruglyak, V. V., Demokritov, S. O. & Grundler, D., Magnonics, *J. Phys. D Appl. Phys.* **43**, 264001 (2010).
- 2 Serga, A. A., Chumak, A. V., & Hillebrands, B. YIG magnonics, *J. Phys. D Appl. Phys.* **43**, 264002 (2010).

- 3 Khitun, A. Bao, M. & Wang, K. L. Magnonic logic circuits. *J. Phys. D Appl. Phys.* **43**, 264005 (2010).
- 4 Lenk, B. *et al.* The building blocks of magnonics. *Phys. Rep.* **507**, 107-136 (2011).
- 5 Krawczyk M. & Grundler D., Review and prospects of magnonic crystals and devices with reprogrammable band structure, *J. Phys.-Cond. Matt.* **26**, 123202 (2014).
- 6 Chumak, A. V. *et al.* Magnon spintronics. *Nat. Phys.* **11**, 453-461 (2015).
- 7 Zografos, O. *et al.* Design and benchmarking of hybrid CMOS-spin wave device circuits compared to 10nm CMOS, *Proc. of the 15th IEEE Int. Conf. on Nanotechn.*, 686-689 (2015).
- 8 Manipatruni, S., Nikonov, D. E. & Young, I. A. Beyond CMOS computing with spin and polarization. *Nat. Phys.* **14**, 338 (2018).
- 9 Chumak, A. V., Fundamentals of magnon-based computing, *arXiv:1901.08934* (2019).
- 10 Duan Z. *et al.* Nanowire spin torque oscillator driven by spin orbit torques, *Nat. Commun.* **5**, 5616 (2014).
- 11 Hahn C. *et al.* Measurement of the intrinsic damping constant in individual nanodisks of Y₃Fe₅O₁₂ and Y₃Fe₅O₁₂/Pt, *Appl. Phys. Lett.* **104**, 152410 (2014).
- 12 Wang, Q. *et al.* Spin pinning and spin-wave dispersion in nanoscopic ferromagnetic waveguides, *arXiv:1807.01358* (2018).
- 13 Sandweg, C. W., *et al.* Spin pumping by parametrically excited exchange magnons, *Phys. Rev. Lett.* **106**, 216601 (2011).
- 14 Yu, H. *et al.* Approaching soft X-ray wavelengths in nanomagnet-based microwave technology, *Nat. Commun.* **7**, 11255 (2016).
- 15 Wintz, S. *et al.* Magnetic vortex cores as tunable spin-wave emitters, *Nat. Nano.*, **11**, 948-953 (2016).
- 16 Brächer, T. *et al.* Detection of short-waved spin waves in individual microscopic spin-wave waveguides using the inverse spin hall effect. *Nano Lett.* **17**, 7234-7241 (2017).
- 17 Liu, C. *et al.* Long-distance propagation of short-wavelength spin waves, *Nat. Commun.* **9**, 738 (2018).
- 18 Kirilyuk, A., Kimel, A.V. & Rasing, T. Ultrafast optical manipulation of magnetic order, *Rev. Mod. Phys.* **82**, 2731 (2010).
- 19 Kampfrath, T. *et al.* Coherent terahertz control of antiferromagnetic spin waves. *Nature Photon.* **5**, 31-34 (2011).
- 20 Qin, H. J. *et al.* Long-living terahertz magnons in ultrathin metallic ferromagnets, *Nat. Commun.* **6**, 6126 (2015).
- 21 Cheng, R. *et al.* Antiferromagnetic spin wave field-effect transistor. *Sci. Rep.* **6**, 24223 (2016).

- 22 Kajiwara, Y. *et al.* Transmission of electrical signals by spin-wave interconversion in a magnetic insulator. *Nature* **464**, 262-266 (2010).
- 23 Dubs, C. *et al.* Sub-micrometer yttrium iron garnet LPE films with low ferromagnetic resonance losses. *J. Phys. D Appl. Phys.* **50**, 204005 (2017).
- 24 Yu, H. *et al.* Magnetic thin-film insulator with ultra-low spin wave damping for coherent nanomagnonics. *Sci. Rep.* **4**, 6848 (2014).
- 25 Evelt M. *et al.* Emission of coherent propagating magnons by insulator-based spin-orbit-torque oscillators, *Phys. Rev. Appl.* **10**, 041002 (2018).
- 26 Demidov, V. E. *et al.* Nonlinear propagation of spin waves in microscopic magnetic stripes. *Phys. Rev. Lett.* **102**, 177207 (2009).
- 27 Krivosik, P. & Patton, C. E. Hamiltonian formulation of nonlinear spin-wave dynamics: Theory and applications. *Phys. Rev. B* **82**, 184428 (2010).
- 28 Chumak, A. V., Serga, A. A., & Hillebrands, B. Magnon transistor for all-magnon data processing. *Nat. Commun.* **5**, 4700 (2014).
- 29 Sadvnikov, A. V. *et al.* Nonlinear spin wave coupling in adjacent magnonic crystals. *Appl. Phys. Lett.* **109**, 042407 (2016).
- 30 Wang, Q. *et al.* Integrated magnonic half-adder, *arXiv:1902.02855* (2019).
- 31 Schneider, T., Serga, A. A. & Hillebrands, B. Realization of spin-wave logic gate. *Appl. Phys. Lett.*, **92**, 022505 (2008).
- 32 Lee, K. -S. *et al.* Conceptual design of spin wave logic gates based on a Mach-Zehnder-type spin wave interferometer for universal logic functions. *J. Appl. Phys.* **104**, 053909 (2008).
- 33 Fischer, T. *et al.* Experimental prototype of a spin-wave majority gate. *Appl. Phys. Lett.* **110**, 152401 (2017).
- 34 Wu, H. *et al.* Magnon valve effect between two magnetic insulators. *Phys. Rev. Lett.* **120**, 097205 (2018).
- 35 Vogt, K. *et al.* Realization of a spin-wave multiplexer, *Nat. Commun.* **5**, 3727 (2014).
- 36 Heussner F. *et al.* Frequency-division multiplexing in magnonic logic networks based on caustic-like spin-wave beams, *Phys. Stat. Sol.* **12**, 1800409 (2018).
- 37 Kozhevnikov, A. *et al.* Pattern recognition with magnonic holographic memory device. *Appl. Phys. Lett.* **106**, 142409 (2015).
- 38 Papp, A. *et al.* Nanoscale spectrum analyzer based on spin-wave interference, *Sci. Rep.* **7**, 9245 (2017).
- 39 Torrejon, J. *et al.* Neuromorphic computing with nanoscale spintronic oscillators. *Nature* **547**, 428-431 (2017).

- 40 Brächer, T. & Pirro, P. An analog magnon adder for all-magnonic neurons. *J. Appl. Phys.* **124**, 152119 (2018).
- 41 Sadovnikov, A. V. *et al.* Directional multimode coupler for planar magnonics: Side-coupled magnetic stripes. *Appl. Phys. Lett.* **107**, 202405 (2015).
- 42 Wang, Q. *et al.* Reconfigurable nanoscale spin-wave directional coupler. *Sci. Adv.* **4**, e1701517 (2018).
- 43 Sebastian, T. *et al.* Micro-focused Brillouin light scattering: imaging spin waves at the nanoscale. *Front. Phys.* **3**, 35 (2015).
- 44 Sadovnikov, A. V. *et al.* Toward nonlinear magnonics: Intensity-dependent spin-wave switching in insulating side-coupled magnetic stripes. *Phys. Rev. B* **96**, 144428 (2017).
- 45 Heussner, F. *et al.* A switchable spin-wave signal splitter for magnonic networks. *Appl. Phys. Lett.* **111**, 122401 (2017).
- 46 Imre, A. *et al.*, Majority logic gate for magnetic quantum-dot cellular automata, *Science* **311**, 205 (2006).
- 47 Verba, R. *et al.* Excitation of propagating spin waves in ferromagnetic nanowires by microwave voltage-controlled magnetic anisotropy. *Sci. Rep.* **6**, 25018 (2016).
- 48 Morozova M. A. *et al.* Suppression of periodic spatial power transfer in a layered structure based on ferromagnetic films, *J. Magn. Magn. Mater.* **466**, **119** (2018).
- 49 Robertson J., Liquid phase epitaxy of garnets, *J. Cryst. Growth* **45**, 233 (1978).
- 50 Maksymov, I. S. & Kostylev, M. Broadband stripline ferromagnetic resonance spectroscopy of ferromagnetic films, multilayers and nanostructures. *Physica E* **69**, 253-293 (2015).
- 51 Vansteenkiste, A. *et al.* The design and verification of MuMax3. *AIP Adv.* **4**, 107133 (2014).
- 52 Kumar, D. *et al.* Numerical calculation of spin wave dispersions in magnetic nanostructures. *J. Phys. D: Appl. Phys.* **45**, 015001 (2012).

Methods

Liquid phase epitaxial film growth and sample fabrication. An 85 nm thick Yttrium Iron Garnet (YIG) film have been grown on 1 inch (111) 500 μm thick Gadolinium Gallium Garnet (GGG) substrate by liquid phase epitaxy from PbO-B₂O₃ based high-temperature solutions at 860°C using the isothermal dipping method (see e.g. Ref. [49]). Nominally pure Y₃Fe₅O₁₂ films with smooth surfaces were obtained on horizontally rotated substrates applying rotation rates of 100 rpm. The saturation magnetization of YIG film is 1.42×10⁵A/m and its Gilbert damping $\alpha = 2.07 \times 10^{-4}$ as was extracted from the ferromagnetic resonance spectroscopy [50].

The directional coupler was fabricated by using electron beam lithography, Ar⁺ ion beam etching and electron beam evaporation. First a double layer of polymethyl methacrylate (PMMA) was spin coated on the YIG film and the directional coupler

structures were created afterwards by using electron beam lithography. To get well shaped waveguides, Titanium and Chromium were deposited by electron beam evaporation as a bilayer hard mask which defines the shape of the directional coupler structures. These were then etched out of the whole film by Ar⁺ ion beam etching. Finally, the U-shaped antenna was defined by using electron beam lithography and lift-off process. It consists of 200 nm thick gold and 20 nm thick titanium (for adhesion).

The fabrication was done in collaboration with the Nano Structuring Center of the Technische Universität Kaiserslautern. A Raith e_Line-System was used for the electron beam lithography, a Pfeiffer Classic 500 L system for the electron beam evaporation and a Roth&Rau IonSys 500 system for the Ar⁺ ion beam etching.

BLS spectroscopy. Micro-focused Brillouin Light Scattering (μ BLS) spectroscopy is a technique for the measurements of spin wave intensities with frequency, space, phase, and time resolution [43]. It is based on inelastic light scattering of the incident laser beam by magnons in a magnetic material. In our measurements, a laser beam of 491 nm wavelength and of a power of 1.8 mW is focused on the directional coupler with an effective spot diameter of 350 nm using a $\times 100$ microscope objective with a large numerical aperture (NA=0.75). The scattered light was collected and guided into a tandem Fabray-Perot interferometer TFP-1 (JRS Scientific Instruments) for further analysis. To perform the two-dimensional scans, the sample was moved with respect to the laser spot in steps of a few hundred nanometer in each direction using a piezoelectric stage.

Calculation of the directional coupler characteristics. The theory of the directional coupler has been described in our previous paper [42]. However, in Ref. [42] we accounted only for the straight part of the coupler where the distance between waveguides is minimal and constant. For the device reported in this article, this approach is not sufficient, since the gap between coupled waveguides is quite large (320 nm). In such a case, the region of the bent waveguides could also significantly contribute to the coupler characteristics, since the gap in this region is not much larger than the minimal gap over a considerable distance. To take this bent region into account, we calculated the splitting of the symmetric and antisymmetric spin wave modes as a function of the gap, $\Delta k = \Delta k(d)$. Then, the coordinate dependence of spin wave power in the waveguides is given by

$$\begin{aligned} P_1(x) &= \cos^2 \left[\int_0^x \frac{1}{2} \Delta k(d(x')) dx' \right], \\ P_2(x) &= \sin^2 \left[\int_0^x \frac{1}{2} \Delta k(d(x')) dx' \right]. \end{aligned} \quad (2)$$

Furthermore, an additional coupling, which is especially pronounced for large spin wave wavelengths, must be taken into account due the large wavelength studied in this work: The part of the first waveguide located before the second one geometrically starts also contributes to the coupling “diagonally”. Indeed, the dynamic magnetization of a large spin wave wavelength varies slowly and, thus, the mentioned part of the first waveguide creates a non-negligible dipolar field at the beginning of the second one. In contrast, for short wavelength spin waves, these additional contributions vanish, because contributions from neighboring half-wavelength parts almost cancel each other. In this work, we account for it by the introduction of an “additional effective length” of the coupler which, by itself, depends on the spin wave wavelength. Since the strength of the dipolar fields decays with the distance approximately proportional to x^{-3} , the effective length is expected to depend on spin wave wavenumber as $L_{\text{eff}} = C_1 / (k + C_2)^2$.

Here, the second power in spin wave wavenumber comes from the integration $\int_0^{1/k} (x + d_0)^{-3} dx$ and the constant C_2 reflects the fact that the effective length cannot increase infinitely for an infinitely large spin wave wavelength. By fitting the experimental

data, we found $C_1 = 25 \mu\text{m}^{-1}$ and $C_2 = 2 \mu\text{m}^{-1}$. Using this expression for the effective additional length, both, frequency and field dependencies of the power transmission rates are well described (see Fig. 1d and Fig. 2b).

The variation of the power transmission rate in the coupler with increasing spin wave power is mainly attributed to the nonlinear frequency shift of the symmetric and antisymmetric spin wave modes in coupled waveguides, as shown in Fig. 3b. The shift of the dispersion results in a change of spin wave wavenumbers at given frequency and, consequently, in a change of the coupling between the waveguides. Knowing the frequency dependence of the power transmission rates $P_{1,2}^{(\text{lin})}(\omega)$ in the linear

regime, the nonlinear characteristics can be calculated simply as $P_{1,2}^{(\text{nl})}(\omega, a) = P_{1,2}^{(\text{lin})}(\omega - T|a|^2)$, where a is the spin wave

amplitude and T is the nonlinear frequency shift ($T/2\pi = -1.8 \text{ GHz}$ in our case [47]). Since experimental data measured for 0 dBm excitation power also corresponds to a weakly nonlinear regime, for the description of power dependence we use the relation

$P_{1,2}^{(\text{nl})}(\omega, a) = P_{1,2}^{(0)}\left(\omega - T\left(|a|^2 - |a_0|^2\right)\right)$, where $P_{1,2}^{(0)}$ - dependence for 0 dBm (measured and fitted by calculations above) and

a_0 - spin wave amplitude at 0 dBm excitation power. The relation of the spin wave amplitude with the excitation power was obtained by measuring the BLS intensity in the first waveguide before the coupler and fitting one adjusting parameter (ratio of BLS counts to the square of spin wave amplitude). We get the following relation $a = 0.035\sqrt{1 + p/17.4}$, where p is the excitation power in dBm. The appearance of an almost linear dependence of the spin wave power on p , instead of an exponential one, which could be expected, is mediated by the strong variation of the spin wave group velocity with spin wave wavenumber, and, consequently, with the excitation power at given frequency. The described simple model fits the experimental data well for the applied powers below 10 dBm (see Fig. 3a). For the higher powers, higher-order nonlinear effects should be taken into account additionally [48].

Micromagnetic simulation. The micromagnetic simulations were performed by the GPU-accelerated simulation program Mumax3 to calculate the space- and time-dependent magnetization dynamics in the investigated structures using a finite-difference discretization [51]. The following material parameters are used: The saturation magnetization $M_s = 1.33 \times 10^5 \text{ A/m}$ is 94% comparing to the value of the plain film due to the Ar^+ ion beam etching and Gilbert damping is $\alpha = 2 \times 10^{-4}$. A standard exchange constant of YIG $A = 3.5 \text{ pJ/m}$ was assumed. There were three steps involved in the calculation of the spin wave dispersion curve [52]: (i) The external field was applied along the waveguide, and the magnetization was relaxed to a stationary state (ground state). (ii) A sinc field pulse $b_y = b_0 \text{sinc}(2\pi f_c t)$, with oscillation field $b_0 = 1 \text{ mT}$ and cutoff frequency $f_c = 10 \text{ GHz}$, was used to excite a wide range of spin waves. (iii) The spin wave dispersion relations were obtained by performing the two-dimensional fast Fourier transformation (FFT) of the time- and space-dependent data.